Chlorpromazine affects glioblastoma bioenergetics by interfering with pyruvate kinase M2

Claudia Abbruzzese
IRCCS - Regina Elena National Cancer Inst., Rome, Italy
Silvia Matteoni
IRCCS - Regina Elena National Cancer Inst., Rome, Italy
Paola Matarrese
Istituto Superiore di Sanita https://orcid.org/0000-0001-5477-3752
Michele Signore
Istituto Superiore di Sanità https://orcid.org/0000-0002-0262-842X
Barbara Ascione
Istituto Superiore di Sanita
Elisabetta Iessi
Istituto Superiore di Sanità
Aymone Gurtner
IRCCS - Regina Elena National Cancer Institute
Andrea Sacconi
IRCCS, Regina Elena National Cancer Institute
Lucia Ricci-Vitiani
Istituto Superiore di Sanità
Roberto Pallini
Catholic University
Andrea Pace
IRCCS - Regina Elena National Cancer Institute
Veronica Villani
IRCCS - Regina Elena National Cancer Institute
Andrea Polo
Istituto Nazionale Tumori-IRCCS-Fondazione G. Pascale
Susan Costantini
Istituto Nazionale Tumori-IRCCS-Fondazione G. Pascale
Alfredo Budillon
Istituto Nazionale Tumori IRCCS Fondazione G. Pascale https://orcid.org/0000-0002-6330-6053
Gennaro Ciliberto
National Cancer Institute, Regina Elena https://orcid.org/0000-0003-2851-8605
Marco G Paggi (✉ marco.paggi@ifo.it)

IRCCS - Regina Elena National Cancer Inst., Rome, Italy https://orcid.org/0000-0002-9445-442X

Article

Keywords: Glioblastoma, Drug repurposing, Chlorpromazine, Bioenergetics, PKM2

Posted Date: March 10th, 2023

DOI: https://doi.org/10.21203/rs.3.rs-2585631/v1

Abstract

Glioblastoma (GBM) is the most frequent and lethal brain tumor, whose therapeutic outcome - only partially effective with current schemes - places this disease among the unmet medical needs, and effective therapeutic approaches are urgently required. In our attempts to identify repositionable drugs in glioblastoma therapy, we identified chlorpromazine (CPZ) as a very promising compound. Here we aimed to further unveil the mode of action of this drug. We performed a supervised recognition of the signal transduction pathways potentially influenced by CPZ via Reverse-Phase Protein microArrays (RPPA) and carried out an Activity-Based Protein Profiling (ABPP) followed by Mass Spectrometry (MS) analysis to possibly identify cellular factors targeted by the drug. Indeed, the glycolytic enzyme PKM2 was identified as a major target of CPZ. Furthermore, using the Seahorse platform, we analyzed the bioenergetics changes induced by the drug. CPZ hindered GBM anabolic pathways and stimulated autophagy. Consistent with the ability of CPZ to target PKM2, we detected relevant changes in GBM energy metabolism, possibly attributable to the drug's ability to inhibit the oncogenic properties of PKM2. RPE-1 non-cancer neuroepithelial cells appeared resistant to the drug. PKM2 silencing reduced the effects of CPZ. 3D modeling showed that CPZ interacts with PKM2 tetramer in the same region involved in binding other known activators. The effect of CPZ can be epitomized as an inhibition of the Warburg effect and, thus, malignancy in GBM cells while sparing RPE-1 cells. These preclinical data enforce the rationale that allowed us to investigate the role of CPZ in GBM treatment in an ongoing multicenter Phase II clinical trial.

Introduction

Glioblastoma (GBM) is the most common and malignant primary brain tumor in adults (1). Even when treated using the best available therapeutic protocol, GBM is associated with a median overall survival of 14.6 months and a 5-year survival <5% (2), denoting an unmet medical need. Frequent clinical relapses of GBM are due to a) its highly invasive nature (3); b) the difficulties of surgical removal (4); c) the existence of different cell subsets of progenitor and glioma stem cells that resist to and adapt under therapeutic pressure (5-7); and d) the ability to build functional networks able to invade the surrounding parenchyma and repair, when damaged, interconnected cancer cells (8). Therefore, novel, effective therapeutic approaches are quite difficult to design but urgently needed.

Drug repurposing, the discipline that discovers new applications for old drugs, allows effective medications to be brought from bench to bedside and seems applicable to GBM (9); antipsychotic drugs play an important role in this setting (10), also according to the recent identification of tumor-neuron synaptic connectivity through which GBM cells use neuromediators as oncogenic stimuli (11). Recently, we investigated the effect of the neuroleptic drug chlorpromazine (CPZ) in inhibiting several molecular and cellular parameters in GBM cells (12, 13), thus paving the way for repurposing this drug in GBM therapy in combination with the first-line therapeutic approach described in 2005 by Stupp *et al.* (2).

CPZ is a safe drug listed in the 2021 WHO Model List of Essential Medicines (current version) (14). It achieves its pharmacological effect in psychiatric disorders by non-specific interference with several CNS neurotransmitter receptors (10, 15). To delve into the mode of action of CPZ, especially as a potential anticancer drug, we undertook two proteomics approaches a) Reverse-Phase Protein microArrays (RPPA) to evaluate the effects of the drug on signal transduction pathways and b) activity-based protein profiling (ABPP) followed by mass spectrometry (MS) analysis, to identify potential hitherto unknown molecular targets. Our data accurately defined the interference of CPZ in modifying major signal transduction pathways and suggested a role for CPZ in interfering with the cellular factor pyruvate kinase (PK) M2. PKM2 is a PK variant that represents a distinctive trait for many cancers and is pivotal for the orchestration of metabolic changes, epitomized as the Warburg effect (16-18).

Results

CPZ alters pivotal signal transduction pathways in GBM cells

The genomic complexity of GBM makes it extremely difficult to predict therapeutic vulnerabilities based only on molecular analyses at a genetic level. Indeed, at a steady state and under environmental pressures, the large spectrum of genomic lesions results in the functional downstream integration of several aberrant signaling pathways in individual GBM patients. Therefore, we sought to use the RPPA to analyze the pathway-level effects of CPZ on GBM cells. To this end, we selected 49 endpoints (The list of the antibodies employed is available as **raw data**, see below**)**, mainly implicated in autophagy and metabolism, and measured the effects of CPZ treatment in GBM cells *in vitro*.

Interestingly, consistent with the biological diversity of GBM, we found that CPZ treatment either hindered or fueled diverse targets in individual cell lines (**Figure 1** and **Figure S1**). Nonetheless, regardless of the dose or timing of the effects produced in anchorage-dependent GBM cells and neurospheres, CPZ treatment led to increased autophagic response, i.e., increased phosphorylation of LKB1 pS428, AMPK-a pT172 and Ac-CoA Carboxylase pS79 (**Figure 1A**), consistent with our previous report (13), and a concomitant reduction of signaling targets involved in the PI3K–mTOR metabolic network, resulting, in particular, in an early decrease of phosphorylated AKT pT308 (2 h) and ultimately of c-Myc levels (8 h). Of note, the levels of phosphorylated AKT were substantially decreased by CPZ **(Figure 1B**). Finally, we found that several analyzed targets showed co-regulation patterns in a cell- and time-dependent manner, further demonstrating the complex signaling network scenario of GBM (**Figure S1**).

Identification of cellular factors as putative targets of CPZ in GBM

Along with RPPA, we employed ABPP+MS to intercept cellular factors as potential direct targets of CPZ in GBM cells. Experiments conducted using a kinase enrichment procedure via an insoluble ATP probe allowed us to identify, by MS analysis, the PKM2 isoform in the U-87 MG GBM cells and TS#1 neurospheres as a factor whose binding to ATP was hindered by the addition of increasing CPZ concentrations (**Figure S2 A-C**).

These results uncovered a potential interference of CPZ with the PKM2 isoform of PK. To validate these results, we analyzed the effects of CPZ on several cellular and molecular processes involving PKM2.

Interference of CPZ with GBM energy metabolism

Since PK is a key regulatory enzyme of the glycolytic pathway, we determined the glycolytic rate in the anchorage-dependent U-87 MG and U-251 MG GBM cell lines using the glycolytic rate acute stress test (ECAR and OCR) performed on a Seahorse XFp platform. This technology allows real-time measurement of the derivative of the amount of H^+ ions released from cells, which is assumed to represent the extracellular lactate concentration. Representative graphs are shown in **Figure 2**. After baseline determination, cells were additioned sequentially with CPZ (red lines) or solvent for control (black lines), rotenone (which blocks ATP production from NADH oxidation) plus antimycin A (AA, a mitochondrial electron transport inhibitor) and, finally, with 2-deoxy-D-glucose (2-DG, a glycolytic poison). In all controls, rotenone plus AA elicited the glycolytic reserve, i.e., the glycolytic boost to compensate for the pharmacologically-induced collapse of ATP production. Finally, the addition of 2-DG dropped the glycolytic rate. As far as ECAR was concerned, the addition of CPZ produced a significant and immediate glycolytic impairment in the U-87 MG and U-251 MG cells, further rendering them less sensitive to the glycolytic boost induced by rotenone plus AA. On the other hand, RPE-1 neuro-epithelial non-cancer cells appeared substantially unaffected by CPZ (**Figure 2A**). The drug also inhibited OCR in U-87 MG and U-251 MG GBM cells, while this parameter was unchanged in the RPE-1 non-cancer cells (**Figure 2B**).

These results outline the ability of CPZ to swiftly interfere with ECAR and OCR in GBM cells while affecting the RPE-1 cells to a lesser extent.

CPZ increases intracellular pyruvate amount in GBM cells

Subsequently, we investigated whether the impairment in GBM lactate production elicited by CPZ was associated with a concomitant variation in the intracellular amount of pyruvate. For this purpose, we incubated GBM cells in the presence of CPZ (or vehicle for controls) for 10 min for the U-87 MG, U-251 MG and RPE-1 cells and 20 min for the TS#1 and TS#163 neurospheres. Cells were washed, lysed, and then the pyruvate amount was determined enzymatically. As a reference, in the same experimental set, cells were incubated with DASA-58, a small molecule known to act as an allosteric activator of PKM2 by inducing its tetramerization and, consequently, its enzyme activity within the glycolytic pathway, thus increasing intracellular pyruvate amount (19). Exposure to CPZ or DASA-58 significantly increased intracellular pyruvate content in all four GBM cells, whereas no significant variations were observed in RPE-1 non-cancer cells (**Figure 3**).

These results concerning extracellular lactate release and intracellular pyruvate amount evoke an active role of CPZ in reprogramming glucose catabolism in GBM cells, likely via an allosteric activation (tetramerization) of PKM2. Overall, a decrease in the Warburg effect could be envisaged.

CPZ decreases nuclear PKM2 amount in GBM cells

We then evaluated CPZ-dependent changes in nuclear PKM2 amounts by confocal microscopy. We measured the mean fluorescence intensity of PKM2 signal in the nuclei following 48 h CPZ treatment. **Figure 4** shows representative images of anchorage-dependent U-87 MG and U-251 MG GBM cells, TS#1 and TS#163 neurospheres and RPE-1 non-cancer cells, after staining with a fluorescent anti-PKM2 MoAb (green) and with DAPI to highlight nuclei (blue), respectively. For each cell line, PKM2 and merged PKM2 + DAPI staining in control cells and CPZ-treated cells is also shown. As a functional control, cells were also treated for 24 h with 30 mM DASA-58, which, as expected (19), reduced nuclear PKM2 amount likely by inducing its tetramerization. Histograms represent the average evaluation of PKM2 nuclear content in ≥150 nuclei for CTL and CPZ and ≥80 for DASA-58-treated cells. A significant nuclear PKM2 reduction was apparent for all the cell lines after treatment with CPZ or DASA-58. Notably, RPE-1 cells displayed an overall lower amount of nuclear PKM2 in untreated cells.

Effect of CPZ on the functional role of nuclear PKM2

A. CPZ alters the transcriptional pattern downstream of nuclear PKM2.

Dimeric PKM2 can translocate into the nucleus, where it associates with various transcription factors (20, 21). PKM2 downstream transcription pattern appeared modified when GBM cells were exposed to CPZ. In detail, *c-MYC* transcription appeared significantly down-regulated in 4/4 (U-87 MG, U-251 MG, TS#1 and TS#163) and *CCND1* in 2/4 (U-87 MG and TS#163) GBM cell lines. Being both *c-MYC* and *CCND1* mRNA expression under direct transcriptional control of PKM2 (22, 23), these results provide a functional link between CPZ and decreased PKM2 nuclear localization. In RPE-1 cells, no significant effects were detectable (**Figure 5A**).

B. CPZ influences nuclear PKM2 kinase activity.

Nuclear PKM2 phosphorylates STAT3 at the Y705 residue, which in turn activates *MEK5* transcription, thus promoting oncogenesis (21, 24). Although CPZ did not affect total amounts of STAT3 protein in exposed GBM cells, western blot analysis showed a significant decrease in STAT3 pY705 (**Figure 5B**). These results are in line with both reduced PKM2 protein kinase activity and decreased amounts of PKM2 in the nuclear compartment. In the RPE-1 cell line, STAT3 protein, though expressed, appeared undetectable in its phosphorylated form. Representative western blot analyses of STAT3 and STAT3 pY705 in control and CPZ-treated cells are shown in **Figure S3**.

PKM2 is a relevant target of CPZ

To further investigate the interference of CPZ with PKM2 nuclear activity, we silenced PKM2 expression in two GBM cells (U-87 MG and TS#163) and assessed its nuclear activity. As compared to control siRNA, PKM2 silencing resulted in a remarkable reduction of PKM2 protein expression in U-87 MG GBM cells, in TS#163 neurospheres and in RPE-1 non-cancer cells, as evaluated via western blotting and RT-PCR (**Figure S4**). Under these conditions, we exposed U-87 MG and TS#163 GBM cells, either siRNA-control or PKM2-silenced, to CPZ and assessed gene expression of *CCND1*, *cMYC,* and also the STAT3 downstream

gene *MEK5*. While CPZ downregulated the expression of these genes in siRNA control cells, the effect of the drug was significantly lower in siRNA-PKM2 cells. *CCND1*, *cMYC,* and *MEK5* transcription in RPE-1 cells was less influenced by PKM2 silencing (**Figure 5C**). In all evaluated cases, the expression fold-changes in PKM2-silenced cells are referred to the corresponding untreated cells.

The clear drop of CPZ-dependent effects in siRNA-PKM2 GBM cells, points to PKM2 as a major cellular target of CPZ in these cells.

CPZ binds PKM2 tetramer in the same binding pocket used by other known activators

To identify the PKM2 amino acid residues that interact with the activators in the binding pocket, we analyzed *in silico* all the experimental structures related to PKM2 tetramer, complexed with activators already reported in PDB, to identify the PKM2 amino acid residues interacting with the activators in the binding pocket. This analysis evidenced that each PKM2 monomer binds a fructose 1,6-bisphosphate (FBP) molecule at an allosteric site located between three amino acid regions (431-437, 482-489, 514-522). In contrast, all the synthetic activators bind to another allosteric site located at the dimer interface of PKM2 and distinct from the FBP binding site (**Table S2**).

Molecular docking simulations were performed as reported in Materials and Methods. The more energetically stable structure of the obtained complex showed that two CPZ molecules fit into the binding pocket of the other activators (**Figure 6A**). Moreover, the protein-drug interaction appeared stabilized by four hydrophobic interactions, two H-bonds, four p-stacking interactions, and a halogen bond (**Figure 6B**).

Indeed, by comparing our CPZ/PKM2 complex with those already reported in PDB for other compounds, we can underline that the affinity energy of our complex falls within the range of values obtained for most complexes and higher only in the case of activators composed by a larger number of atoms and functional groups. Finally, our complex has the maximum number of π-stacking interactions compared with known PDB structures, as the CPZ molecule is a polycyclic aromatic compound containing a linear tricyclic system consisting of two benzene rings joined by a para-thiazine ring (**Table S3**).

Therefore, these results demonstrated a specific interaction between two CPZ molecules and PKM2 and support the ability of the drug to act as a PKM2 allosteric activator.

Discussion

Drug repurposing has been investigated in GBM treatment (9, 25, 26), also considering antipsychotic drugs (10, 27-29) that possess the added value of pharmacokinetic characteristics that allow them to freely cross the blood–brain barrier. Our data help establish the potential anticancer role of CPZ and highlight PKM2 as a novel target for this medication.

Our results show that PKM2 has a pivotal role in cancer cell bioenergetics, ultimately governing the Warburg effect, i.e., the high glucose consumption and lactate production that most cancer cells display even in the presence of adequate oxygen concentrations and intact cellular machinery devoted to

mitochondrial ATP production (16, 22, 23, 30). Warburg effect is also essential for protecting cancer stem cells from their elevated ROS production (31).

Our results highlight the ability of CPZ to interfere with GBM energy metabolism and key signal transduction pathways involved in the anabolic processes used by these cells to facilitate the synthesis of building blocks for biomass generation.

The overall picture of these modifications indicates the ability of CPZ to slow down cellular anabolism attributable to a possible energy shortage (see below) and to elicit a stress response in GBM cells, which stimulate an autophagic pathway in search for rescue strategies, in line with previous findings (13, 32).

Indeed, the effects of CPZ described here in impairing the PI3K/mTOR pathway, activating autophagy, and reducing lactate production seem attributable to the interaction we recognized between the drug and PKM2. Of note, the CPZ-induced decrease in extracellular acidification could radically modify the peritumoral environment and make it less fit for cancer growth and progression (33). In GBM cells, CPZ behaved very similarly to the PKM2 allosteric activator DASA-58, a compound known to favor the tetrameric form of PKM2 and consequently reduce its nuclear content and the Warburg effect. DASA-58 impedes cancer cell growth in preclinical *in vitro* and *in vivo* models (34); however, we are unaware of clinical trials involving this molecule or other known tetrameric PKM2 activators in GBM therapy. In this context, the advantage of CPZ derives from its status as a repositionable drug, a medication widely used mainly for the therapy of neuropsychiatric disorders. This makes this compound eligible for prompt use in clinical experimentation.

Noticeably, CPZ appeared less toxic for the RPE-1 non-cancer cells. A reason to explain the selective toxicity of CPZ toward GBM cells could be envisaged in the peculiar pattern of expression of PK isoforms postulated for cancer cells, where a higher PKM2/PKM1 ratio is widely described. Indeed, PKM2 tetrameric activators operate to favor the generation of a tetramer from two PKM2 dimers and have no described effect on PKM1 or other PK isoforms constitutively present as a tetramer. Therefore, these drugs do not modify PK activity sustained by PKM1 or other isoforms in cells expressing negligible or null amounts of PKM2 (34, 35), allowing us to assume that PKM1 could safeguard non-cancer cells. Conversely, PKM2 tetramerization can hinder major GBM malignant features (34).

We should also consider that no related toxicity has been described in psychiatric patients undergoing long-term therapy with CPZ at high doses. Incidentally, there are anecdotal reports of a reduced cancer incidence in patients under therapy with CPZ (36) and a better GBM clinical course in psychiatric patients on neuroleptics (37).

The results reported here show the multiple pharmacodynamic activities of CPZ, hindering the survival ability of GBM cells while displaying less toxicity toward the RPE-1 non-cancer neuroectodermal cells.

On this basis, we initiated a Phase II clinical trial, approved by our Institutional Ethics Committee (Comitato Etico Centrale IRCCS - Sezione IFO-Fondazione Bietti, Rome, Italy) on September 6, 2019

(EudraCT # 2019-001988-75; ClinicalTrials.gov Identifier: NCT04224441). In this ongoing trial, CPZ has been added to the standard GBM treatment in patients carrying a tumor with a hypo-methylated *MGMT* gene and thus characterized by resistance to TMZ and poorer prognosis. The dose of CPZ administered to GBM patients is 25-50 mg/day for 6 months during the adjuvant phase of the first-line treatment and in concomitance with the routine TMZ schedule (38). The results of this trial will be available in March 2023. Another Phase I clinical trial (ClinicalTrials.gov Identifier: NCT05190315) is currently investigating the use of CPZ throughout the standard of care for GBM therapy.

Since the whole process required to develop and bring new drugs to clinics is currently extremely long and expensive (39, 40), experimental and clinical investigators are strongly motivated to consider drug repositioning/repurposing (41), especially now that novel bioinformatics and multi-omics platforms can help unveil the potential of several well-known medications. This approach may also provide further benefits, including safety, a faster track to clinical use and a relative inexpensiveness, with the aim to provide novel and effective therapeutic approaches for GBM patients.

Methods

Cell lines

Anchorage-dependent GBM cell lines U-87 MG and U-251 MG, anchorage-independent TS#1 and TS#163 neurospheres, and anchorage-dependent hTERT-immortalized human retinal pigment epithelial cells hTERT RPE-1 (henceforth RPE-1) are described and cultured as previously reported (13).

Drugs

CPZ was purchased as “Largactil” from Teofarma S.R.L., Valle Salimbene (PV), Italy, as a 25 mg/ml solution (78 mM). CPZ doses used throughout the paper refer to the IC30 for each cell line, as determined by their 48-h exposure to the drug (see **Table S1**, where IC50 doses are also reported). DASA-58 was purchased as a powder from Selleckchem, Houston, TX, USA, and dissolved in DMSO as a 50 mM stock solution.

RPPA

Anchorage-dependent GBM cells U-251 MG, U-87 MG, and TS#1 and TS#163 neurospheres were seeded onto 6-well microtiter plates (3.5×10^3 cells/well) and treated either with vehicle or CPZ at the cell line-specific IC30 and IC50 for 2 and 8 h and processed as described (42-44). Cells from three different passages were used for biological replicates of individual experimental conditions.

Identification of potential CPZ protein targets

To identify potential cellular targets of CPZ, we employed ABPP in competitive mode. Multiple aliquots of the same native GBM cell lysates were incubated with increasing concentrations of CPZ (5-40 μM) and then mixed with an ATP-mimicking insoluble probe. Proteins whose ATP-binding ability was influenced by

the drug were picked and identified by MALDI-MS and MS/MS analysis. All these procedures were performed as described (45).

Evaluation of metabolic parameters

A. Oxygen consumption rate (OCR) and extracellular acidification rate (ECAR)

OCR and ECAR measurements were performed using the Seahorse XFp Real-Time Cell metabolic analyzer (Agilent Technologies, Santa Clara, CA 95051, USA) following manufacturer's instructions (**Supplementary Materials and Methods**).

B. Intracellular Pyruvate determination

The amount of intracellular pyruvate was determined using the enzymatic Pyruvate Kinase Activity Assay MAK072 from Sigma-Aldrich Merck KGaA, Darmstadt, Germany, following manufacturer's instructions (**Supplementary Materials and Methods**).

RNA extraction and RT-PCR

U-87 MG and U-251 MG anchorage-dependent cells and TS#1 and TS#163 neurospheres were treated with CPZ for 24 h, while control cells were treated with the same volume of vehicle. Total RNA was extracted using miRNeasy Extraction Kit (QIAGEN, Hilden, Germany), and RNA concentration was determined. After reverse RNA transcription, real-time (RT) polymerase chain reaction (PCR) analyses were performed to determine PKM2 downstream transcriptional activity. All RT-PCR data were quantified using the $2^{-\Delta\Delta CT}$ method, and CT values were normalized to GAPDH. Values represent fold changes related to control cells, arbitrarily reported as 1.0.

Primers are described in **Supplementary Materials and Methods**.

Confocal microscopy

The procedures implemented for confocal microscopy are described in **Supplementary Materials and Methods**.

siRNA Transfection

U-87 MG GBM cells and RPE-1 non-cancer cells were seeded in 35-mm diameter dishes; on the following day, cells were transfected with 10 nM siRNA-PKM2 (siPKM2) or negative control siRNA using Lipofectamine RNAiMAX (Invitrogen Thermo Fisher Scientific). Small interfering-PKM2 (PKM2 Silencer Select Validated siRNA) and negative control siRNA (Silencer Select Negative Control #1 siRNA) were purchased from Ambion (Austin, TX, USA). After 48-h transfection, cells were treated with CPZ or vehicle for 24 h, collected, and used for RT-PCR and/or western blot analysis.

TS #163 neurospheres were plated in Stem Medium containing 3% Matrigel (Corning Matrigel Growth Factor Reduced Basement Membrane Matrix, Merck, Darmstadt, Germany); the subsequent day, cells underwent PKM2 silencing as described above for anchorage-dependent cells.

Molecular docking simulations

To predict CPZ's best binding to the tetrameric PKM2 structure, molecular docking studies were performed using AutoDock 4.2.6 tool (46) and employing the crystal structure of the PKM2 tetramer (PDB code: 5X1W) as the target (47) and CPZ structure retrieved from ZINC20 database as the ligand [https://pubs.acs.org/doi/10.1021/acs.jcim.0c00675]. The docking protocol was performed by extracting a co-crystallized ligand and docking two CPZ molecules into the active pocket in each PKM2 dimer. See **Supplementary Materials and Methods** for further details.

The 10 best poses of each CPZ molecule were clustered using an RMSD value <2.0 Å. The best-docked conformation of two CPZ molecules on two dimers of PKM2 was selected in the obtained cluster based on the binding affinity (expressed in kcal/mol) and the number of ligand–protein interaction residues, H-bonds, salt bridges, and hydrophobic and stacking interactions by AutoDock4.2.6 (46), LIGPLOT (48), PLIP (49) and PRODIGY (50).

Statistical analysis

Three independent experiments were carried out for confocal microscopy images, and statistical analysis was performed, on ≥150 nuclei for CTL and CPZ and ≥80 for DASA-58-treated cells, using an unpaired Student's *t*-test (Prism v9, GraphPad Software Inc., San Diego, CA).

Pyruvate concentrations and transcription levels expression determinations are described as mean±Standard Deviation (SD). Up- or down-regulations relative to controls were analyzed using the Student's two-tailed *t*-test (Prism v9, GraphPad Software Inc.). Asterisks denote statistical significance (*p<0.05; **p<0.01; ***p<0.001).

Declarations

Acknowledgments

This paper is dedicated to the memory of our friend and colleague Armando Felsani, who recently passed away and who contributed so much to the advancement of knowledge in the field of cell differentiation and cell cycle regulation.

The human immortalized RPE-1 cell line was courtesy of Giulia Guarguaglini, CNR, Rome, Italy. Sergio Visentin, ISS, Rome, has been of invaluable help in setting up the early experiments with the Seahorse platform.

Editorial and graphical assistance were provided by Aashni Shah, Valentina Attanasio and Massimiliano Pianta (Polistudium SRL, Milan, Italy), and was supported by internal funds.

Conflict of Interest

The authors declare no conflict of interest.

Author contributions

Conceptualization and design: CA, SM, PM, MS, APa, VV, APo, SC, AB, GC, MGP; Development of methodology: CA, SM, PM, MS, AG, LRV, APo, SC, AB, MGP; Resources: CA, SM, PM, MS, LRV, RP, APa, VV, APo, SC, AB; Data acquisition: CA, SM, PM, MS, BA, EI, AG, APo, SC, Bioinformatical analysis: CA, PM, MS, AS, APo, SC; Visualization: CA, SM, PM, MS, APo, SC, AB, MGP; Writing—original draft: CA, SM, PM, MS, APa, MGP; Writing— review and editing: CA, SM, PM, MS, APa, AB, GC, MGP; Supervision: CA, APa, AB, GC, MGP; Funding acquisition: MGP, PM.

Funding

Work partially financed by Funds Ricerca Corrente 2018-2019, 2020-2021, 2022-2023 from Italian Ministry of Health (MGP) and by the European Union – Next Generation EU – PNRR M4C2 – Investment 1.3 via MUR (MGP).

Data Availability

Raw data are available at the following link:

https://gbox.garr.it/garrbox/index.php/s/5Cg4hKZ5DQNsKss

References

1. McNeill KA. Epidemiology of Brain Tumors. Neurol Clin. 2016;34(4):981-98.
2. Stupp R, Mason WP, van den Bent MJ, Weller M, Fisher B, Taphoorn MJ, et al. Radiotherapy plus concomitant and adjuvant temozolomide for glioblastoma. N Engl J Med. 2005;352(10):987-96.
3. Rao JS. Molecular mechanisms of glioma invasiveness: the role of proteases. Nat Rev Cancer. 2003;3(7):489-501.
4. Glas M, Rath BH, Simon M, Reinartz R, Schramme A, Trageser D, et al. Residual tumor cells are unique cellular targets in glioblastoma. Ann Neurol. 2010;68(2):264-9.
5. Lan X, Jorg DJ, Cavalli FMG, Richards LM, Nguyen LV, Vanner RJ, et al. Fate mapping of human glioblastoma reveals an invariant stem cell hierarchy. Nature. 2017;549(7671):227-32.
6. Gimple RC, Bhargava S, Dixit D, Rich JN. Glioblastoma stem cells: lessons from the tumor hierarchy in a lethal cancer. Genes Dev. 2019;33(11-12):591-609.

7. Couturier CP, Ayyadhury S, Le PU, Nadaf J, Monlong J, Riva G, et al. Single-cell RNA-seq reveals that glioblastoma recapitulates a normal neurodevelopmental hierarchy. Nat Commun. 2020;11(1):3406.
8. Osswald M, Jung E, Sahm F, Solecki G, Venkataramani V, Blaes J, et al. Brain tumour cells interconnect to a functional and resistant network. Nature. 2015;528(7580):93-8.
9. Abbruzzese C, Matteoni S, Signore M, Cardone L, Nath K, Glickson JD, et al. Drug repurposing for the treatment of glioblastoma multiforme. J Exp Clin Cancer Res. 2017;36(1):169.
10. Persico M, Abbruzzese C, Matteoni S, Matarrese P, Campana AM, Villani V, et al. Tackling the Behavior of Cancer Cells: Molecular Bases for Repurposing Antipsychotic Drugs in the Treatment of Glioblastoma. Cells. 2022;11(2):263.
11. Venkataramani V, Schneider M, Giordano FA, Kuner T, Wick W, Herrlinger U, et al. Disconnecting multicellular networks in brain tumours. Nat Rev Cancer. 2022.
12. Matteoni S, Matarrese P, Ascione B, Buccarelli M, Ricci-Vitiani L, Pallini R, et al. Anticancer Properties of the Antipsychotic Drug Chlorpromazine and Its Synergism With Temozolomide in Restraining Human Glioblastoma Proliferation In Vitro. Front Oncol. 2021;11:635472.
13. Matteoni S, Matarrese P, Ascione B, Ricci-Vitiani L, Pallini R, Villani V, et al. Chlorpromazine induces cytotoxic autophagy in glioblastoma cells via endoplasmic reticulum stress and unfolded protein response. J Exp Clin Cancer Res. 2021;40(1):347.
14. World Health Organization Model List of Essential Medicines, 22nd List. Geneva: World Health Organization; 2021.
15. Barygin OI, Nagaeva EI, Tikhonov DB, Belinskaya DA, Vanchakova NP, Shestakova NN. Inhibition of the NMDA and AMPA receptor channels by antidepressants and antipsychotics. Brain Res. 2017;1660:58-66.
16. Wiese EK, Hitosugi S, Loa ST, Sreedhar A, Andres-Beck LG, Kurmi K, et al. Enzymatic activation of pyruvate kinase increases cytosolic oxaloacetate to inhibit the Warburg effect. Nat Metab. 2021.
17. Palsson-McDermott EM, Curtis AM, Goel G, Lauterbach MA, Sheedy FJ, Gleeson LE, et al. Pyruvate kinase M2 regulates Hif-1alpha activity and IL-1beta induction and is a critical determinant of the warburg effect in LPS-activated macrophages. Cell Metab. 2015;21(1):65-80.
18. Liang J, Cao R, Zhang Y, Xia Y, Zheng Y, Li X, et al. PKM2 dephosphorylation by Cdc25A promotes the Warburg effect and tumorigenesis. Nat Commun. 2016;7:12431.
19. Almouhanna F, Blagojevic B, Can S, Ghanem A, Wolfl S. Pharmacological activation of pyruvate kinase M2 reprograms glycolysis leading to TXNIP depletion and AMPK activation in breast cancer cells. Cancer Metab. 2021;9(1):5.
20. Zhou Z, Li M, Zhang L, Zhao H, Sahin O, Chen J, et al. Oncogenic Kinase-Induced PKM2 Tyrosine 105 Phosphorylation Converts Nononcogenic PKM2 to a Tumor Promoter and Induces Cancer Stem-like Cells. Cancer Res. 2018;78(9):2248-61.
21. Gao X, Wang H, Yang JJ, Liu X, Liu ZR. Pyruvate kinase M2 regulates gene transcription by acting as a protein kinase. Mol Cell. 2012;45(5):598-609.

22. Wong N, Ojo D, Yan J, Tang D. PKM2 contributes to cancer metabolism. Cancer Lett. 2015;356(2 Pt A):184-91.
23. Yang W, Zheng Y, Xia Y, Ji H, Chen X, Guo F, et al. ERK1/2-dependent phosphorylation and nuclear translocation of PKM2 promotes the Warburg effect. Nature cell biology. 2012;14(12):1295-304.
24. Yu H, Lee H, Herrmann A, Buettner R, Jove R. Revisiting STAT3 signalling in cancer: new and unexpected biological functions. Nat Rev Cancer. 2014;14(11):736-46.
25. Basso J, Miranda A, Sousa J, Pais A, Vitorino C. Repurposing drugs for glioblastoma: from bench to bedside. Cancer Lett. 2018.
26. Tan SK, Jermakowicz A, Mookhtiar AK, Nemeroff CB, Schurer SC, Ayad NG. Drug Repositioning in Glioblastoma: A Pathway Perspective. Front Pharmacol. 2018;9:218.
27. Cheng HW, Liang YH, Kuo YL, Chuu CP, Lin CY, Lee MH, et al. Identification of thioridazine, an antipsychotic drug, as an antiglioblastoma and anticancer stem cell agent using public gene expression data. Cell Death Dis. 2015;6:e1753.
28. Elmaci I, Altinoz MA. Targeting the cellular schizophrenia. Likely employment of the antipsychotic agent pimozide in treatment of refractory cancers and glioblastoma. Crit Rev Oncol Hematol. 2018;128:96-109.
29. Abbruzzese C, Matteoni S, Persico M, Villani V, Paggi MG. Repurposing chlorpromazine in the treatment of glioblastoma multiforme: analysis of literature and forthcoming steps. J Exp Clin Cancer Res. 2020;39(1):26.
30. Nandi S, Razzaghi M, Srivastava D, Dey M. Structural basis for allosteric regulation of pyruvate kinase M2 by phosphorylation and acetylation. J Biol Chem. 2020;295(51):17425-40.
31. Sebastian C, Ferrer C, Serra M, Choi JE, Ducano N, Mira A, et al. A non-dividing cell population with high pyruvate dehydrogenase kinase activity regulates metabolic heterogeneity and tumorigenesis in the intestine. Nat Commun. 2022;13(1):1503.
32. Shin SY, Lee KS, Choi YK, Lim HJ, Lee HG, Lim Y, et al. The antipsychotic agent chlorpromazine induces autophagic cell death by inhibiting the Akt/mTOR pathway in human U-87MG glioma cells. Carcinogenesis. 2013;34(9):2080-9.
33. Corbet C, Feron O. Tumour acidosis: from the passenger to the driver's seat. Nat Rev Cancer. 2017;17(10):577-93.
34. Anastasiou D, Yu Y, Israelsen WJ, Jiang JK, Boxer MB, Hong BS, et al. Pyruvate kinase M2 activators promote tetramer formation and suppress tumorigenesis. Nat Chem Biol. 2012;8(10):839-47.
35. Vander Heiden MG, Christofk HR, Schuman E, Subtelny AO, Sharfi H, Harlow EE, et al. Identification of small molecule inhibitors of pyruvate kinase M2. Biochem Pharmacol. 2010;79(8):1118-24.
36. Csatary LK. Chlorpromazines and cancer. Lancet. 1972;2(7772):338-9.
37. Faraz S, Pannullo S, Rosenblum M, Smith A, Wernicke AG. Long-term survival in a patient with glioblastoma on antipsychotic therapy for schizophrenia: a case report and literature review. Ther Adv Med Oncol. 2016;8(6):421-8.

38. Pace A, Lombardi G, Matteoni S, Villani V, Benincasa D, Abruzzese C, et al. Ctni-12. Phase Ii Multicentric Italian Trial on Repositioning of the Antipsychotic Drug Chlorpromazine and Its Combination with Temozolomide in Mgmt Unmethylated Glioblastoma Patients: The Ractac Trial. Neuro-Oncology. 2022;24(Supplement_7):vii72-vii.
39. Ashburn TT, Thor KB. Drug repositioning: identifying and developing new uses for existing drugs. Nat Rev Drug Discov. 2004;3(8):673-83.
40. Nosengo N. Can you teach old drugs new tricks? Nature. 2016;534(7607):314-6.
41. Langedijk J, Mantel-Teeuwisse AK, Slijkerman DS, Schutjens MH. Drug repositioning and repurposing: terminology and definitions in literature. Drug Discov Today. 2015;20(8):1027-34.
42. Matteoni S, Abbruzzese C, Matarrese P, De Luca G, Mileo AM, Miccadei S, et al. The kinase inhibitor SI113 induces autophagy and synergizes with quinacrine in hindering the growth of human glioblastoma multiforme cells. J Exp Clin Cancer Res. 2019;38(1):202.
43. Signore M, Alfonsi R, Federici G, Nanni S, Addario A, Bertuccini L, et al. Diagnostic and prognostic potential of the proteomic profiling of serum-derived extracellular vesicles in prostate cancer. Cell Death Dis. 2021;12(7):636.
44. Signore M, Manganelli V. Reverse Phase Protein Arrays in cancer stem cells. Methods Cell Biol. 2022;171:33-61.
45. Abbruzzese C, Matteoni S, Persico M, Ascione B, Schenone S, Musumeci F, et al. The small molecule SI113 hinders epithelial-to-mesenchymal transition and subverts cytoskeletal organization in human cancer cells. J Cell Physiol. 2019;234(12):22529-42.
46. Morris GM, Huey R, Lindstrom W, Sanner MF, Belew RK, Goodsell DS, et al. AutoDock4 and AutoDockTools4: Automated docking with selective receptor flexibility. J Comput Chem. 2009;30(16):2785-91.
47. Matsui Y, Yasumatsu I, Asahi T, Kitamura T, Kanai K, Ubukata O, et al. Discovery and structure-guided fragment-linking of 4-(2,3-dichlorobenzoyl)-1-methyl-pyrrole-2-carboxamide as a pyruvate kinase M2 activator. Bioorg Med Chem. 2017;25(13):3540-6.
48. Laskowski RA, Swindells MB. LigPlot+: multiple ligand-protein interaction diagrams for drug discovery. J Chem Inf Model. 2011;51(10):2778-86.
49. Adasme MF, Linnemann KL, Bolz SN, Kaiser F, Salentin S, Haupt VJ, et al. PLIP 2021: expanding the scope of the protein-ligand interaction profiler to DNA and RNA. Nucleic Acids Res. 2021;49(W1):W530-W4.
50. Xue LC, Rodrigues JP, Kastritis PL, Bonvin AM, Vangone A. PRODIGY: a web server for predicting the binding affinity of protein-protein complexes. Bioinformatics. 2016;32(23):3676-8.

Figures

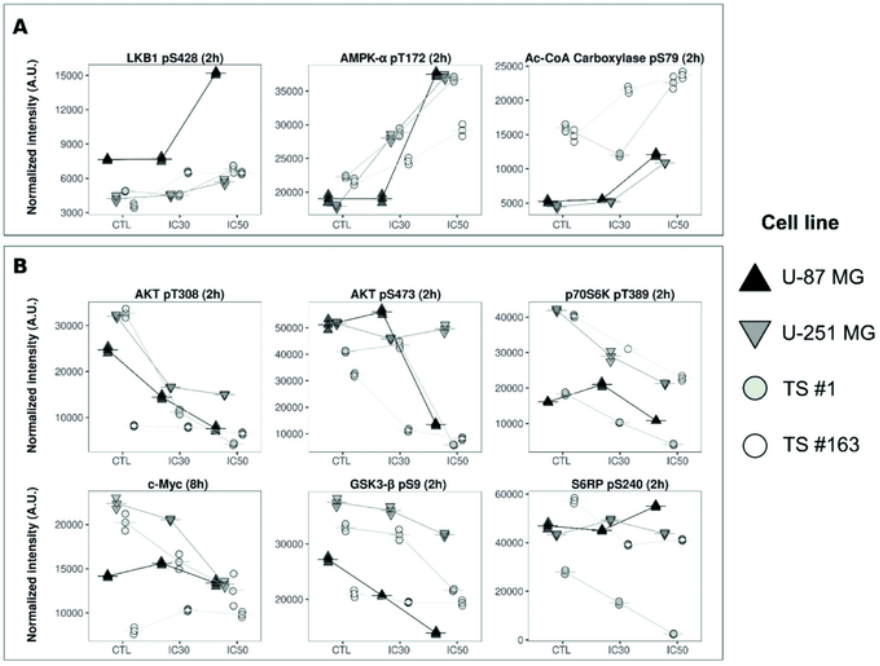

Figure 1

RPPA analysis of anchorage-dependent GBM cells and neurospheres challenged with CPZ. The panels include selected plots of normalized RPPA levels (Arbitrary Units, AU) for (**A**) endpoints implicated in autophagy and (**B**) PI3K-mTOR metabolic network, as measured over a three-point dose response of CPZ (Control, IC30 and IC50, from left to right) at either 2 or 8 h. N=3.

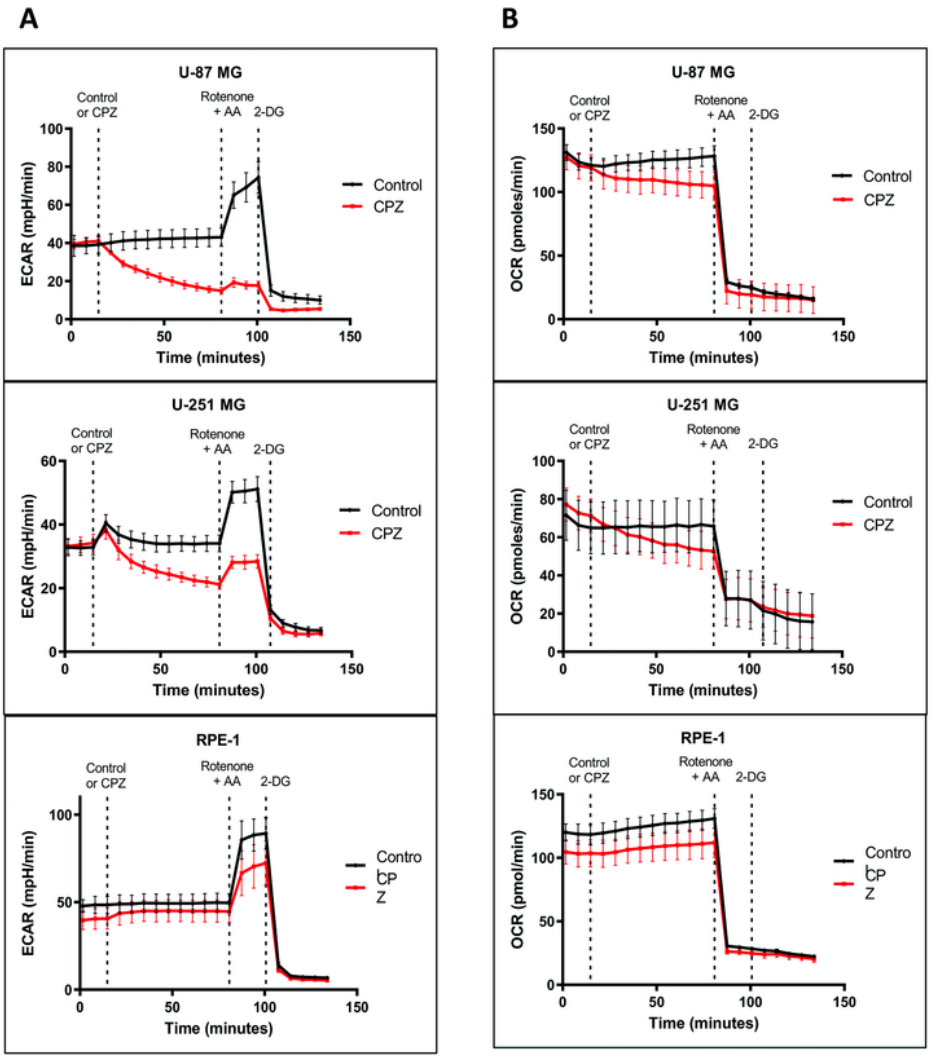

Figure 2

Interference of CPZ with glucose metabolism in GBM cells. Cells were incubated using the Seahorse XFp platform. Dashed vertical lines indicate, from left to right, the time of addition of CPZ or solvent for control, rotenone plus AA and 2-DG, respectively. Red lines represent CPZ-treated cells and black lines control (solvent-treated) cells. **A**. ECAR plots related to U-87 MG, U-251 MG GBM cell lines and RPE-1 non-cancer cells. **B**. OCR plots related to U-87 MG, U-251 MG GBM cell lines and RPE-1 non-cancer cells. All

experiments were performed three times in triplicate. Representative graphs are shown here; dots and vertical bars indicate mean±SD. Raw data from all experiments are available in **Supplementary Material**.

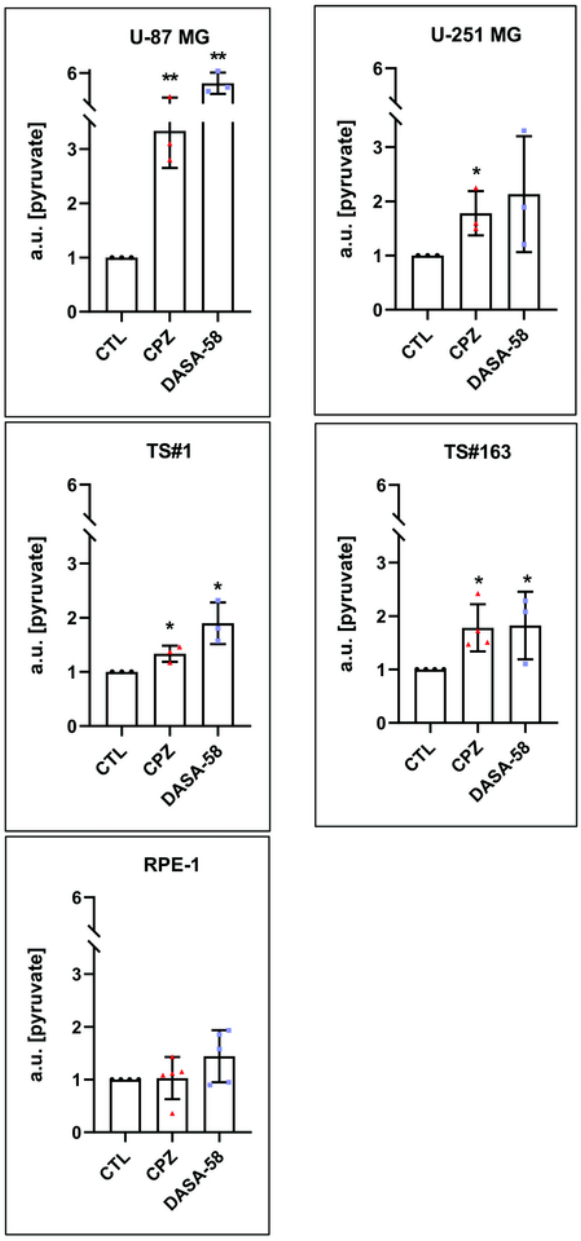

Figure 3

CPZ increases intracellular pyruvate amount in GBM cells. Anchorage-dependent U-87 MG and U-251 MG GBM cells and RPE-1 non-cancer cells were exposed to CPZ or solvent (CTL) for 10 min, while

neurospheres TS#1 and TS#163 were exposed for 20 min. As a reference, all cell lines were exposed, under the same conditions, to 30 mM DASA-58, a known PKM2 activator. Histograms show the amount of intracellular pyruvate expressed in arbitrary units (a.u.). Asterisks denote statistical significance (*p<0.05; **p<0.01). N≥3.

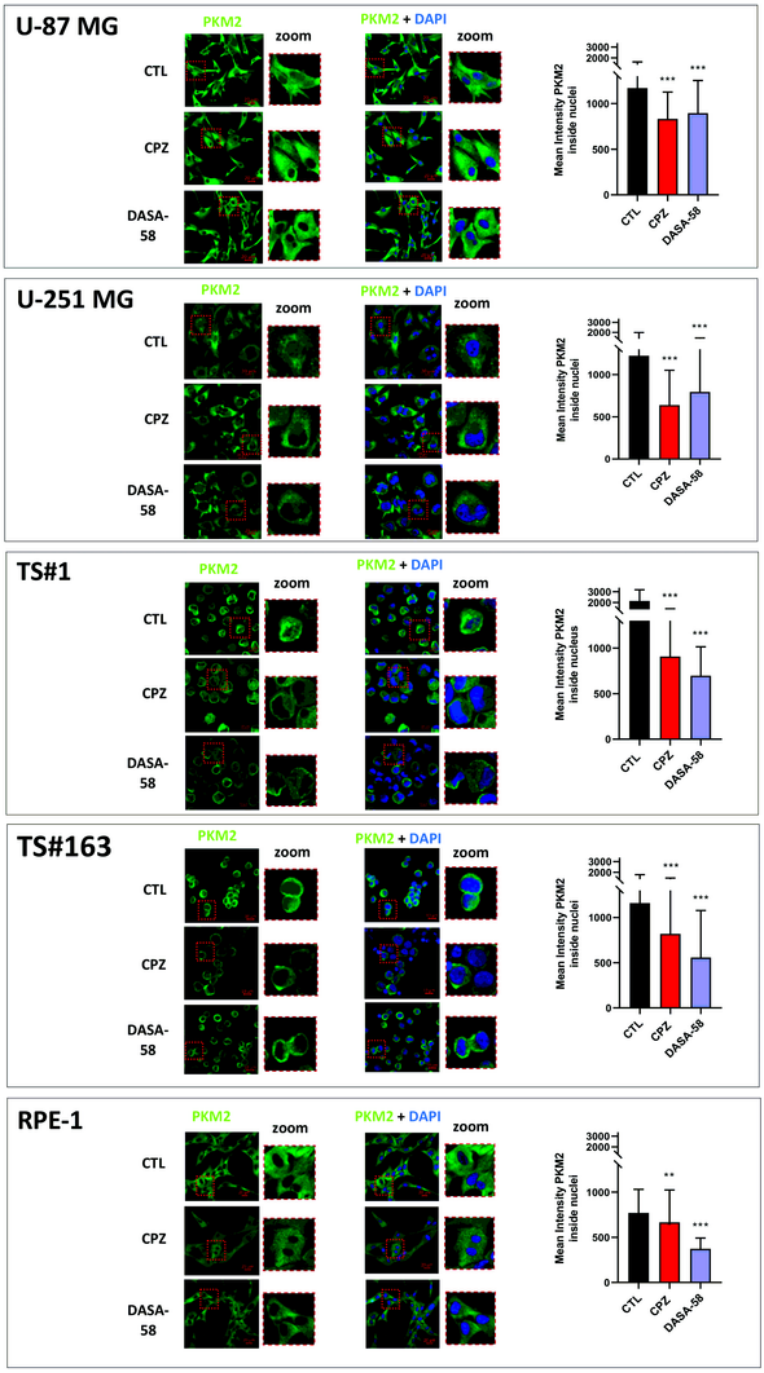

Figure 4

CPZ produces a decrease in nuclear PKM2 concentration in GBM cells. Representative confocal microscopy images of U-87 MG, U-251 MG, TS#1, and TS#163 GBM cell lines and RPE-1 non-cancer cells untreated, CPZ-treated or DASA-58-treated. Green fluorescence shows PKM2, while merging with DAPI (blue) highlights the nuclear structures. The smaller pictures at the right of each image (zoom) reproduce at higher magnification the contents of the red square in each bigger microphotography. Histograms on the right quantify the reduction in nuclear PKM2 mean intensity in CPZ-treated cells (red) or in DASA-58-treated cells (light blue) when compared with controls (black), as evaluated via the microscope software. N≥150 nuclei for CTL and CPZ and ≥80 for DASA-58-treated cells. Scale bars are shown in each microphotography. Asterisks denote statistical significance (*p<0.05; **p<0.01; ***p<0.001).

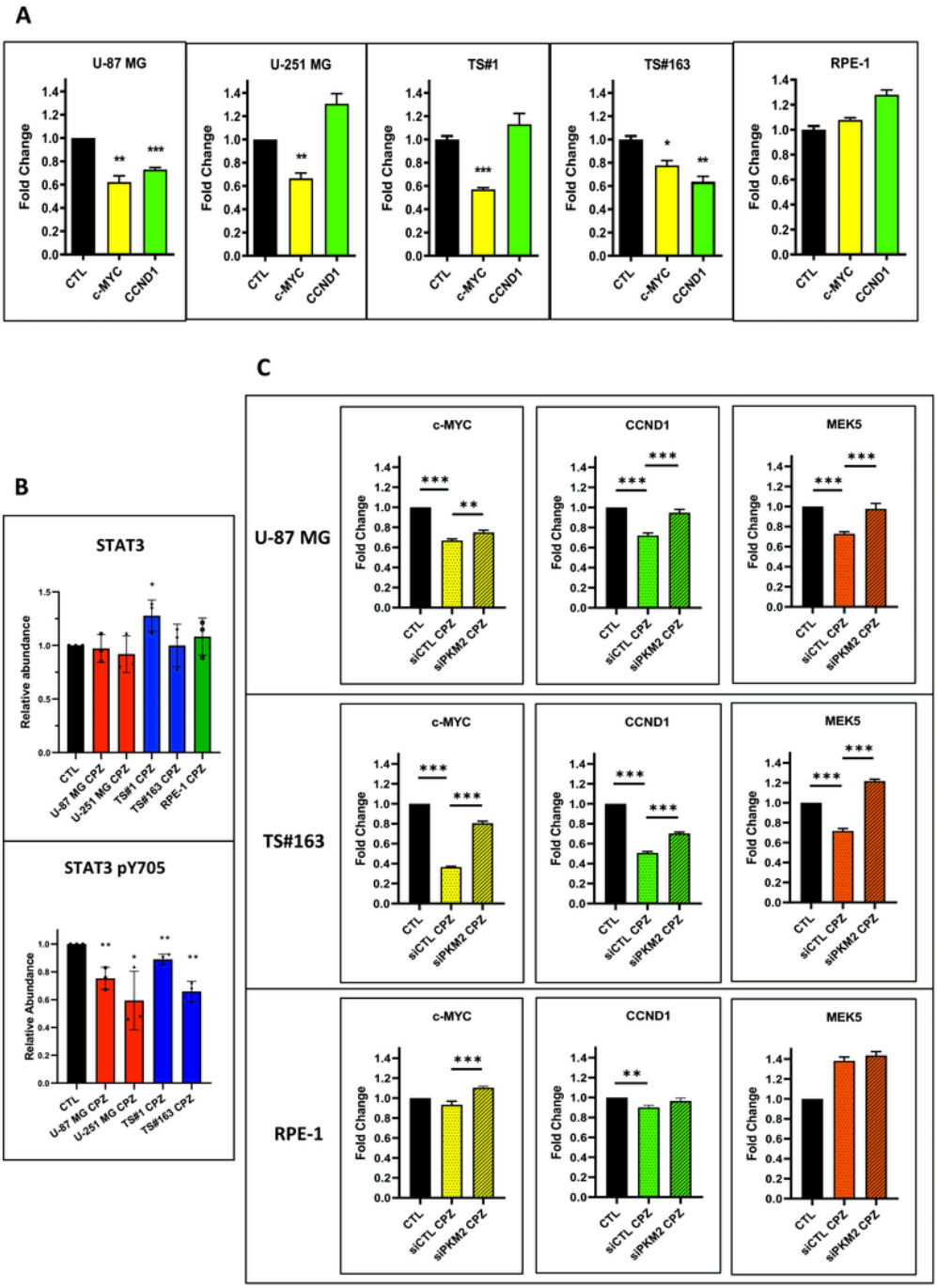

Figure 5

CPZ hinders the function of nuclear PKM2. A. Expression of *c-MYC* and *CCND1* target genes, as assessed by RT-qPCR, in all the GBM cells and in the RPE-1 cell line. N≥10. **B**. STAT3 total protein amount and STAT3 pY705 amount as assessed via western blot in all the GBM cells and in the RPE-1 cell line. N=3. **C**. U-87 MG, TS#163 GBM cells, and RPE-1 non-cancer cells were treated with siRNA Control or siRNA-PKM2 and exposed to CPZ or solvent for control. Histograms indicate the levels of *CCND1*, *c-MYC,* and *MEK5*

mRNA expression, as assessed by RT-qPCR when PKM2 expression was downregulated. The histogram bars related to the control (CTL) values, normalized to 1.0 (solid black), refer to the untreated siRNA Control and PKM2 silenced cells. In all the panels, asterisks denote statistical significance (*p<0.05; **p<0.01; ***p<0.001). N≥10.

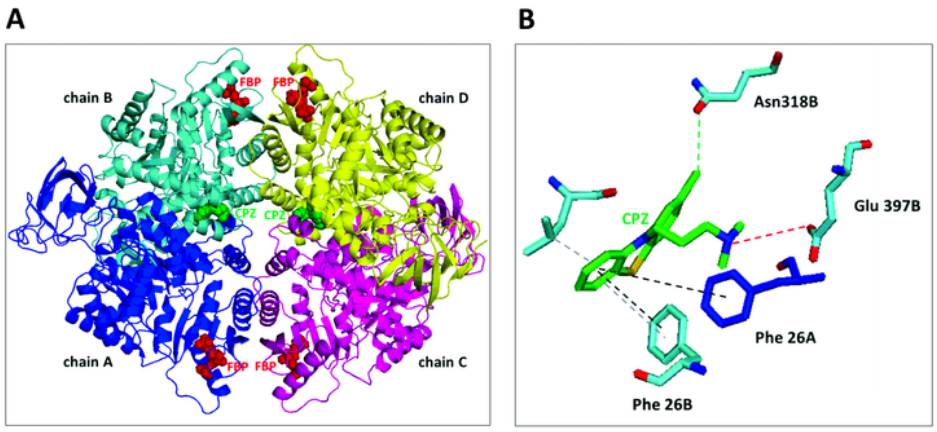

Figure 6

CPZ binds PKM2 tetramer in the same binding pocket of other known activators. A) Molecular structure of the PKM2/CPZ complex. Chain A is shown in blue, chain B in cyan, chain C in magenta, and chain D in yellow. Four FBP and two CPZ molecules are reported as red and green spheres, respectively. **B**) Snapshot of the interaction between chlorpromazine molecule and the chains A and B evidencing stacking and hydrophobic interactions, hydrogen and halogen bonds by dashed black, grey, red, and green lines, respectively.

Supplementary Files

This is a list of supplementary files associated with this preprint. Click to download.

- GAPDHRPE1.tif
- GAPDHTSX1andTSX163up.tif
- GAPDHTSX1andTSX163.tif
- GAPDHU87MGandU251MG.tif
- GAPDHpY705U87MGandU251MG.tif
- RPE1GAPDH.tif
- RPE1Norm.tif
- RPE1PKM2.tif
- RPE1STAT3Y705.tif
- STAT3TOTRPE1.tif
- STAT3TotTSX1andTSX163.tif
- STAT3pY705TSX1TSX163.tif
- STAT3pY705U87MGandU251MG.tif
- STAT3totU87MGandU251MG.tif
- SupplementaryFigures1to4.pdf
- SupplementaryMaterial.docx
- TSX163Norm.tif
- TSX163PKM2.tif
- U87MGNorm.tif
- U87MGPKM2.tif